UNDERSTANDING FIBER/MATRIX INTERFACIAL SHEAR STRENGTH MEASUREMENT IN POLYMER-MATRIX COMPOSITES USING PUSH-OUT TEST

Quy Tung Linh Vu[1,2], Guillaume Seon[1*], Sarvenaz Ghaffari[1], Andrew Makeev[1], Frederic Lachaud[2], Miguel Charlotte[2] and Yves Gourinat[2]
[1] The University of Texas at Arlington (UTA), 76019 Arlington TX, USA,
[2] Institut Clément Ader (ICA), DMSM, ISAE-SUPAERO, 31400 Toulouse, France
* Corresponding author (seon@uta.edu)

Keywords: *Residual Stress, Fiber Push-Out, Micromechanics*

ABSTRACT

Accurate assessment of fiber-matrix interfacial shear strength (IFSS) may play a key role in understanding structural strength behavior of polymer-matrix composites and provide additional flexibility for enabling the development of high performing materials and designs. The fiber push-out test is a common micromechanical test method for IFSS measurement where a nano-indenter is used to axially load fibers in thin membrane test samples until debonding/push-out occurs. The recorded force-displacement curve and maximum peak load are then used for evaluation of interfacial shear properties. While the fiber push-out testing procedure is conceptually simple, successful preparation of the test samples, realization of the experiment and interpretation of the results can be challenging. In this work, an experimental study that compares push-out results from test samples prepared using femtosecond laser machining with samples prepared using conventional lapping/polishing is presented to highlight some of the challenges associated with manufacturing high-quality fiber push-out test specimens. In-situ Scanning Electron Microscopy (SEM)-based experiments presented in this work also reveal significant matrix deformation associated with the release of residual stress in resin-rich areas during fiber push-out, which highlights the importance of using in-situ imaging for improved understanding of material response during micro-mechanical testing. Finally, a finite element analysis study is conducted to quantify the effects of matrix properties and residual stress on the push-out response and direct assessment of the interfacial shear strength property.

1 INTRODUCTION

Accurate assessment of fiber-matrix interface shear strength (IFSS) may play a key role in understanding shear, compression, and bearing structural strength behavior of polymer-matrix composites including Carbon Fiber Reinforced Plastics (CFRPs). Shear microbuckling driven fiber-direction compressive strength has been a well-recognized weakness of CFRPs imposing severe limitations on structural performance. In particular, high-modulus (HM) CFRPs have a history of very low compressive strength prohibiting insertion of such materials in aircraft primary structures [1]. In-situ SEM based single fiber push-out tests assessing fiber-matrix interface shear strength have been essential for understanding compressive strength behavior of HM CFRPs and possibly enabling lightweight material designs improving this key property [2,3].

Characterization of the fiber/matrix interface may be achieved through various mechanical testing methods, such as pull-out test, fragmentation test, push-in test and push-out test, wherein the thin-membrane fiber push-out test has been the most widely used technique [4-10]. In the fiber push-out test, a nano-indenter is used to axially load fibers in thin membrane test samples until debonding/push-out occurs at the fiber/matrix interface. The recorded force-displacement curve and maximum peak load are then used for evaluation of interfacial shear properties. The advantage of the fiber push-out test compared to the other methods is the relative simplicity of the testing procedure, in addition to the ability of making a direct measurement of the interface shear strength.

However, while the fiber push-out testing procedure is conceptually simple, successful preparation of the test samples, realization of the experiment and interpretation of the results remain challenging.

The specimen must be thin enough (20-100 μm) to allow decohesion over the entire fiber/matrix interface and ensure complete push-out of the fibers without causing additional damage from unwanted failure modes. Such thin samples are typically prepared by mechanical machining techniques, such as grinding, polishing and/or lapping. These processes are typically time consuming and may introduce unwanted material damage. Additionally, high tolerance in terms of constant membrane thickness and specimen flatness is difficult to achieve using conventional material removal techniques. An alternative method for machining thin-membrane specimens is femtosecond laser ablation. Using femtosecond laser has several advantages including higher cutting speeds, minimum force-induced mechanical damage and absence of abrasives or liquid media [11, 12]. The femtosecond laser ablation process also allows additional flexibility in terms of push-out specimen design, which can be used to overcome challenges related to geometric/flatness imperfections in specimens machined using conventional grinding/polishing methods [2,3].

Fabrication of high-quality fiber push-out test specimens is only one of the requirements for successful assessment of IFSS in CFRPs. Typical carbon fiber diameters range from 5 to 7 micrometers, therefore special equipment is required to ensure accurate placement of the apparatus used to load the fibers in the axial direction and perform push-out. Recent advances in micro and nanoscale testing equipment, including commercialization of scanning electron microscopes (SEM) with integrated micro/nano/pico indenters allowing in situ dynamic high-resolution imaging during testing, are increasing the confidence in the ability to break through the current length scale limits.

Finally, challenges in the interpretation of the test results are worth mentioning. The IFSS is commonly estimated in the push-out test using the formula:

$$IFSS = \frac{P_{max}}{A} = \frac{P_{max}}{2\pi rh} \tag{1}$$

Where h is the membrane thickness of the specimen, r is the fiber radius and P_{max} is the maximum peak load recorded. Equation (1) assumes uniform shear stress over the interface and studies have demonstrated the limitations of this simplification in situations that include material non-linear behavior, membrane bending or imperfect membrane geometry [13]. Process-induced residual stress, if not accounted for, may also affect the accuracy of the IFSS estimation using Equation (1). Microscale residual stress may develop during the curing process of CFRPs due to the mismatch between carbon fibers and epoxy matrix chemical and thermal properties.

This work presents the results of an experimental and numerical study with the objective to improve the understanding of fiber/matrix IFSS measurement using the push-out test in regard to the challenges previously mentioned.

First, experimental data that compares push-out results from test samples prepared using the conventional lapping/polishing method with samples prepared using femtosecond laser machining is presented to highlight the challenges associated with manufacturing high-quality test specimens and demonstrate the advantages of femtosecond laser machining. Second, in-situ SEM-based fiber push-out experiments are presented where significant permanent matrix deformation is observed after groups of neighboring fibers in resin-rich areas are pushed-out. This deformation is associated with the release of residual stress, which highlights the importance of using in-situ SEM imaging for improved interpretation of test data and material response. Finally, a finite element analysis study is conducted to quantify the effects of matrix properties and residual stress on the push-out response and the direct assessment of the interfacial shear strength property using Equation (1).

2 FIBER PUSH OUT EXPERIMENTS

2.1 Test setups and specimen preparation

Two methods and test setups were considered for preparation of thin-membrane test samples for fiber push-out testing, conventional lapping/polishing (free-standing configuration) and femtosecond (fs) laser ablation (cave configuration), as illustrated in Figure 1a and 1b, respectively.

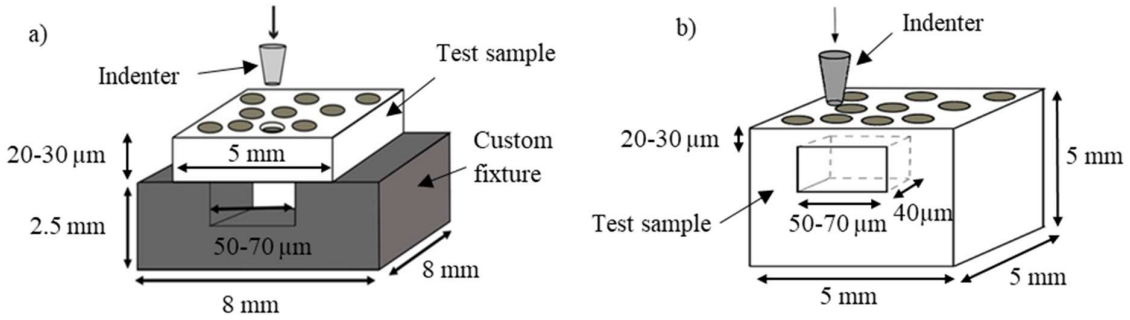

Figure 1: a) Free-standing and b) cave fiber-push out test configurations.

For the free-standing setup, thin-membrane test samples are obtained by lapping/polishing the top and bottom surfaces of small 5x5x5 mm (approximately) sections of material machined from a unidirectional panel until a final sample thickness of 20-30 µm was achieved. Polishing is performed using a sequence of silicon carbide abrasive papers of 320, 600, 800 and 1200 grit with specimens mounted on a disk grinder (Model 623, Gatan) using thermoplastic mounting wax (Crystalbond, Ted Pella). To ensure a quality finish, final polishing was performed with 0.04 µm colloidal silica suspension. The test samples are then mounted on a 2.5 mm thick custom steel fixture with a 50–70 µm wide groove, as illustrated in Figure 1a. The specimens are secured using conductive tape and tested using a PicoIndenter micromechanical load frame with a flat end diamond indenter tip. The load frame is integrated in a scanning electron microscope (SEM) for in situ-monitoring. Figure 2 shows an example of SEM images of a free-standing test sample mounted on the fixture prior to test.

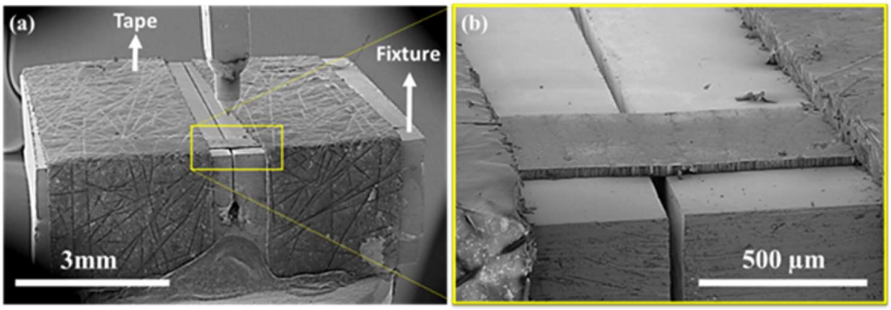

Figure 2: SEM images of a free-standing specimen mounted on the fixture before test.

For the cave setup, the 5x5x5 mm sections of material are polished on one side using the same sequence of silicon carbide papers and colloidal silica suspension. After that, fs-laser machining was performed using a custom apparatus to remove material in the transverse direction and create a milled out section underneath the polished surface, to construct a thin membrane with 20–30 µm thickness, 50–70 µm width and a cutting depth of 40 µm. An example of cave test specimens is shown in Figure 3. The cave specimens are then directly tested using the same a PicoIndenter micromechanical load frame integrated with SEM. For more details on specimen preparation and test procedure, the reader is referred to Ref. [3].

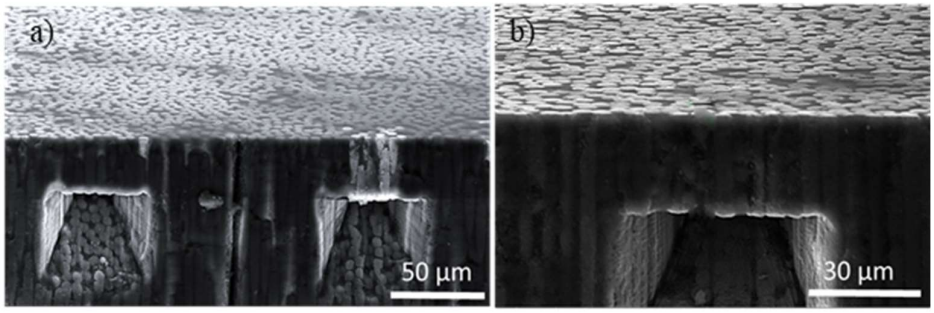

Figure 3: SEM images of a cave specimen before test.

2.3 Test results

Fiber push-out results using both the free-standing and cave test configurations are presented for a HM63/8552 carbon/epoxy material system. HM63 is a 12K-filament-count-tow Polyacrylonitrile (PAN) based high-modulus carbon fiber with diameter of 5µm and 8552 is a 177°C (350°F) curing toughened epoxy resin system both manufactured by Hexcel. Individual fibers are pushed-out using a Thermofisher Quattro SEM equipped with a Bruker PI-88 PicoIndenter micro/nanomechanical load frame with a 4 µm diameter flat-tip conical diamond probe. All fiber push-out tests were conducted under displacement control at a loading rate of 30 nm/s up to the maximum displacement limited to 4000 nm, followed by unloading to the initial position. In the cave configuration, the membrane thickness was approximately 25 µm. For the free-standing configuration, two specimens with membrane thickness of 22 µm and 30 µm, respectively, were considered. Precise loading conditions were monitored by real-time in-situ SEM imaging. If the indenter tip was determined not to be centered on the fiber during the experiment or interface fracture was not the observed failure mode, the data was rejected.

The load-displacement data was recorded and the load P is normalized by the fiber/matrix interface area according to Equation (1). The resulting stress-displacement curves from push-out tests on nine individual fibers in the cave configuration and five fibers in the 22 µm and 30 µm thick free-standing samples are shown in Figure 4. Overall, the IFSS values are in good agreement, with 95.0 MPa (COV 6.0%) for the cave configuration, 89.6 MPa (COV 3.9%) for the 22 µm thick free-standing configuration and 89.2 MPa (COV 2.4%) for the 30 µm thick free-standing configuration.

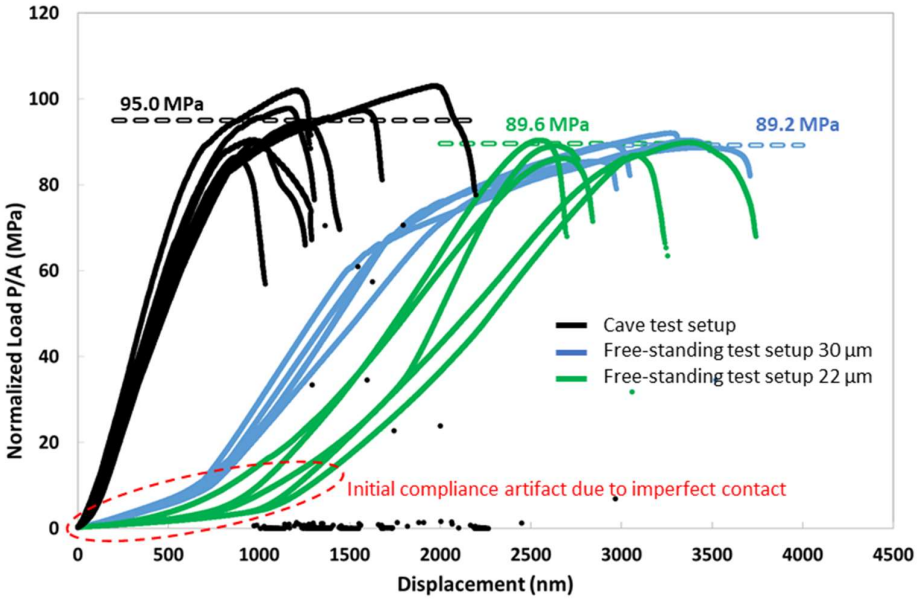

Figure 4: Stress-displacement curves for HM63/8552 cave and free-standing fiber push-out test configurations.

Despite good agreement between the two configurations in terms of peak load, significant differences are visible in the initial load-displacement response. Fibers pushed-out from the cave sample appear to show a material-like stress-displacement response starting from a linear elastic behavior expected from a perfectly bonded interface, followed by a nonlinear response continuing until the peak load is reached. After peak load, a load drop is observed in the load-displacement response, which is associated with rapid propagation of fiber/matrix interface failure resulting in a fiber push-out visible in the in-situ SEM imaging data. On the other hand, free-standing specimens exhibit a highly nonlinear response at small loads well within the range of elastic material response, with high initial compliance and large scatter initial scatter (displacement shift). This behavior is attributed to imperfect contact condition at the interface between the sample and the test fixture, which is likely due to imperfectly flat surfaces. For example, Figure 5 shows a SEM image of a free-standing sample depicting a gap between the specimen and fixture. At the beginning of the test, imperfect contact conditions lead to excessive compliance until full contact is established and the slope of the stress-displacement response increases.

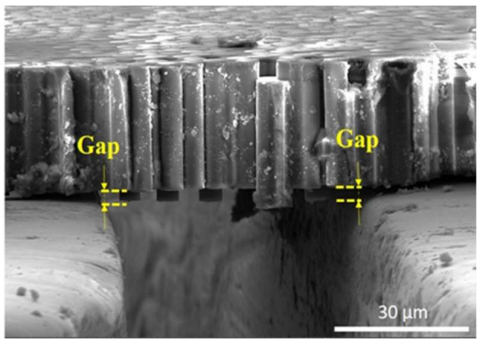

Figure 5: Initial gap between the specimen and test fixture visible in the SEM image of a free-standing test specimen before push-out test.

While certain improvements in the preparation of the free-standing samples may be possible to improve flatness and reduce compliance artifacts and scatter, the stress-displacement response is likely to be representing specimen-specific response rather than material behavior due to high sensitivity to boundary conditions. Potentially, inadequate sample geometry and testing conditions could result in unintended failure modes and interfere with characterization of the interfacial shear properties. Caves specimens are free of such imperfections and seem to be better-suited candidates for assessment of the fiber-matrix interface shear response, including the interface strength.

3 MATRIX SINK-IN DEFORMATION

Live SEM monitoring during the fiber push-out experiment in free-standing specimens revealed visible permanent matrix deformation after fibers are pushed out. This effect was amplified when a group of neighboring fibers in resin-rich areas are pushed out and was attributed in part to the release of process-induced microscale residual stress. Residual stress develops during the curing process due to property mismatch between fibers and matrix, including thermal and cure properties. For instance, the chemical shrinkage strain of epoxy resins used in CFRPs is commonly of the order of several percent [14,15] while carbon fibers are typically inert at the curing temperature and their chemical shrinkage is comparatively negligible. During the cooldown phase of the curing process, additional residual stress might also build up due to the difference in Coefficient of Thermal Expansion (CTE) between fibers and matrix. The CTE of common epoxies is around 50 ppm/°C, while the CTE of common carbon fibers used in aerospace CFRPs application is typically negative and of two orders of magnitude smaller. Stiff continuous carbon fibers constrain matrix shrinkage in the fiber direction after curing and temperature cool down, leading to built-up of tensile residual stress. Once the fiber/matrix interface is broken, residual tensile stresses are released leading to matrix "sink-in" deformation, as illustrated in Figure 6.

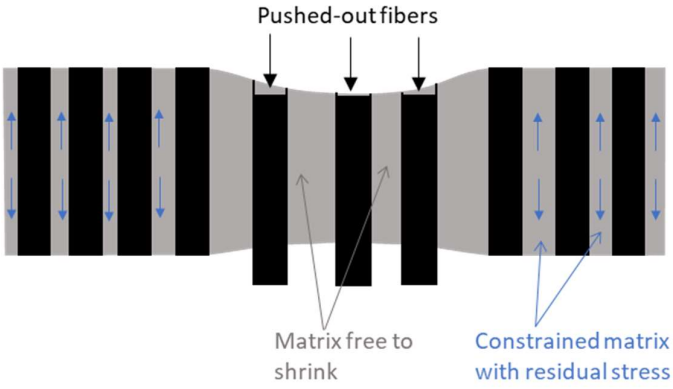

Figure 6: Release of residual stress and matrix "sink-in" deformation after pushing out a group of fibers.

Figure 7 shows an example of matrix sink-in deformation observed in a resin-rich area in a free-standing specimen using SEM imaging after two groups of fibers are successively pushed-out. Figure 7a shows the specimen before local push out. In Figure 7b, 11 fibers have been pushed out and an additional group of 7 fibers has been pushed out in Figure 7c. Careful high-resolution inspection of the fiber push-out area using SEM imaging did not reveal any visible signs of matrix damage or local plastic deformation, which supports the assumption that the permanent deformation observed is related to the release of residual stresses. The sink-in deformation in the out-of-plane direction was quantified by probing the same location at the center of the resin rich area with the indenter tip before the test (Figure 7a), after pushing the first group of fibers (Figure 7b) and after pushing the second group of fibers (Figure 7c).

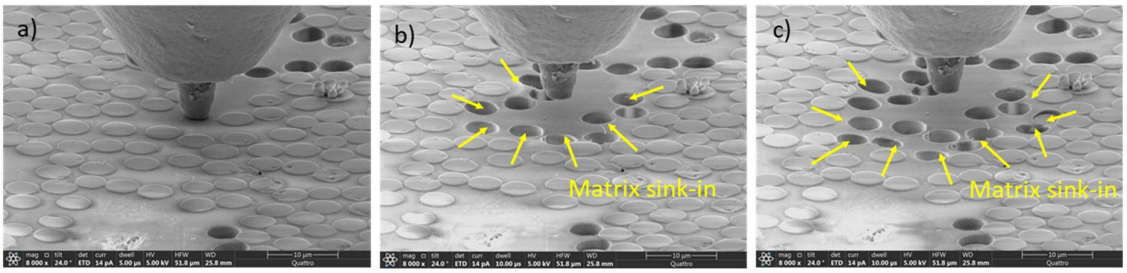

Figure 7: Experimental observation of matrix sink-in using SEM imaging in a free-standing specimen: a) prior to push-out, b) after pushing the first group of 11 fibers and c) after pushing an additional group of 7 fibers.

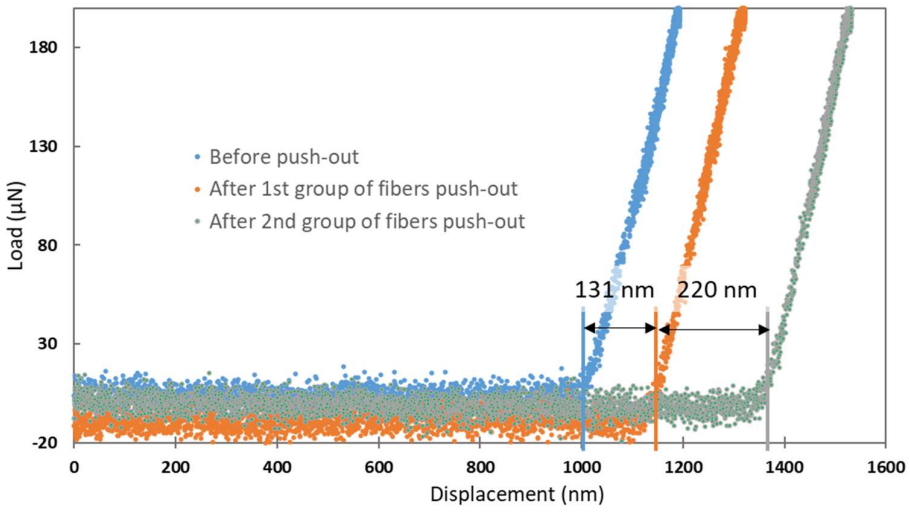

Figure 8: Load-displacement data recorded during indentation probing for evaluation of matrix sink-in deformation.

Figure 8 shows the load-displacement data recorded during indentation probing. The sharp inflection point in the load-displacement data indicates that the probe is touching the matrix and the recorded displacement at this point is used to determine the absolute position of the probe. Once the load reached about 200 μN the indentation test was interrupted, and the probe was lifted. The same "zero-displacement" reference is used for the three recordings, which allows measurement of the matrix out-plane deformation before and after push-out test. As shown in Figure 8, the sink-in out-of-plane deformation was 131 nm after the first group of fibers are pushed out; and the push-out of the second group resulted in an additional 220 nm of matrix shrinkage. The total sink-in deformation recorded was 351 nm, which corresponds to about 1.5% of the specimen thickness (22.8 μm).

Similar experiments were conducted on different resin-rich areas and additional samples, leading to total matrix sink-in deformation ranging between 260-360 nm (1.0-1.6% of specimen thickness). Such range of deformation is significant, suggesting high levels of residual stress. High residual stress, in combination with other effects such as matrix non-linear response and interface friction could potentially interfere with measurement of the interface shear strength properties during the push out test. The following section presents the result of a finite element analysis based sensitivity study to evaluate such effects and improve understanding of the fiber push-out response in CFRPs.

3 FINITE ELEMENT ANALYSIS

3.1 Finite element models

FE micromodels representative of the free-standing configuration are used for sensitivity analysis, with an example shown in Figure 9. As illustrated in Figure 9, the FE model is fiber-segmented, and a random fiber distribution is considered. The fiber volume fraction in this example is approximately 60%, which is representative of the materials considered. The 60% fiber volume fraction is achieved using a modified Random Sequential Adsorption (RSA) algorithm for insertion of non-overlapping circles into a rectangular shape, similar to the algorithm used in [16]. The FE models are created for Abaqus FEM analysis. The probe and the fixture are modelled using analytical rigid surfaces. The fiber and matrix materials are represented for the most part using 3D brick elements C3D8R from Abaqus library, with a few 6-nodes reduced integration prismatic C3D6 elements.

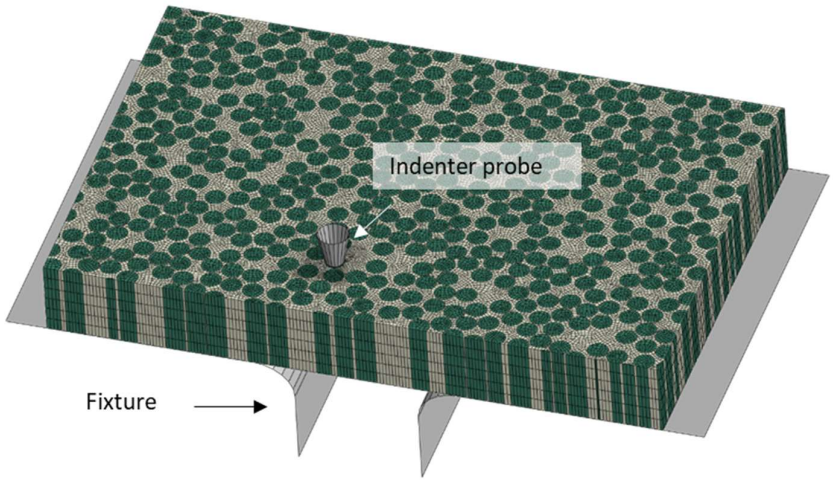

Figure 9: Fiber-segmented FE model of a free-standing specimen and fixture for simulation of fiber push-out.

A refined embedded mesh region is created for the area around the selected pushed-out fiber in order to accurately capture stress concentrations and local deformations as well as fiber-matrix debonding. The embedded refined mesh is connected to the coarser mesh representing the rest of the specimen using tie constraints, as illustrated in Figure 10. The interface between the pushed-out fiber and the surrounding matrix in the embedded mesh region is represented using Abaqus built-in cohesive contact model for simulation of interface debonding. The reference membrane thickness and fiber diameter were 24.5 µm and 5 µm, respectively, which is representative of the test specimens presented in the previous section. The total number of degrees of freedom in the FE models was between 0.5M-1M. Convergence of the results with mesh refinement was verified for all the simulation results presented in the following sections.

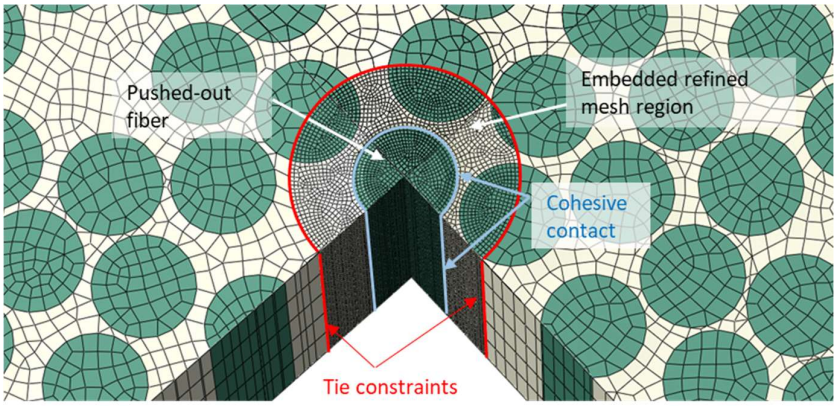

Figure 10: Embedded region with higher mesh density in the pushed-out fiber area.

The fiber material is modeled using linear-elastic orthotropic constitutive properties. The matrix material is represented as an isotropic material with a Drucker-Prager damage-plasticity model available in Abaqus library of built-in material models. A quadradic strength-based mixed-mode initiation criterion and a linear damage evolution law based on the Benzeggagh-Kenane (BK) mixed-mode fracture criterion are used for the cohesive model representing the fiber-matrix interface. Baseline constitutive properties representative of HS40/F3G carbon/epoxy material listed in Table 1 are used in this study. HS40 is a Mitsubishi 12K-filament-count-tow Polyacrylonitrile (PAN) based high modulus carbon fiber with diameter of 5µm. F3G is a 121°C (250°F) curing toughened epoxy resin system manufactured by Patz Materials and Technologies (PMT).

HS40 single carbon fiber properties	
Longitudinal Young's Modulus E_{11}, GPa	455
Transverse Young's Modulus $E_{22} = E_{33}$, GPa	13
Poisson's ratio $v_{12} = v_{13}$	0.3
Poisson's ratio v_{23}	0.46
Shear Modulus $G_{12} = G_{12}$, GPa	11.3
Shear Modulus G_{23}, GPa	4.45
Coefficient of thermal expansion CTE, ppm/°C	-0.7
F3G epoxy resin properties	
Young's Modulus E, GPa	4.3
Poisson's ratio v	0.3
Tensile yield strength, MPa	121
Compressive yield strength, MPa	176
Internal friction angle β, degrees	29
Fracture toughness, N/mm	0.1
Coefficient of thermal expansion CTE, ppm/°C	42.7
Fiber/matrix interface properties	
Normal cohesive strength t_n, GPa	75
Shear cohesive strength $t_s = t_t$, GPa	95
Mode I fracture toughness G_{IC}, N/mm	0.002
Mode II&III fracture toughness G_{IIC}, N/mm	0.05
BK coefficient	1.45

Table 1: Mechanical properties for HS40/F3G carbon-epoxy material.

3.2 Effects of matrix plasticity properties

A benchmark FE model similar to the model shown in Figures 9 & 10 and representative of a free-standing sample with random fiber distribution at 60% fiber volume fraction is considered to study the effects of matrix plasticity properties of the fiber push-out response. The sensitivity parameters selected are the tensile and compressive yield strengths of the Drucker-Prager damage-plasticity model used for the constitutive response of the epoxy matrix. Load-displacement results are shown in Figure 11 & 12 for the effects of the tensile and compressive yield strengths, respectively. Reference parameters and other material properties used in the model are listed in Table 1. The load-displacement results in Figures 11 & 12 are compared to the "ideal" closed-form solution for P_{max} given by Equation (1) with an IFSS input property of 95 MPa used as shear cohesive strength in the cohesive model for the fiber/matrix interface.

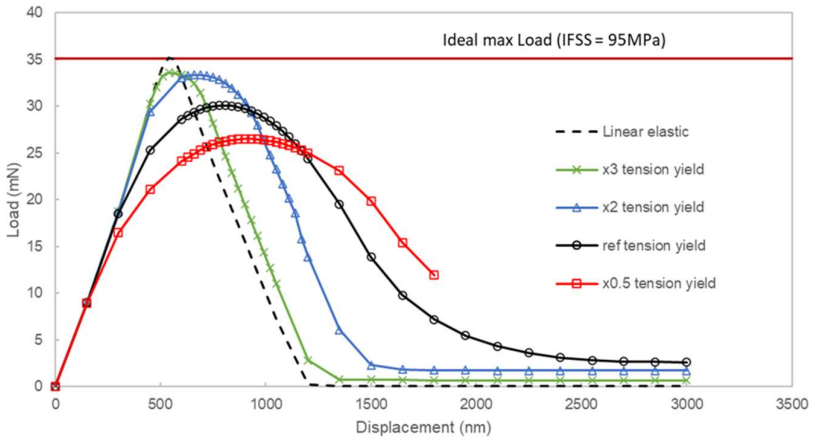

Figure 11: Effects of tensile yield strength on fiber push-out load-displacement response.

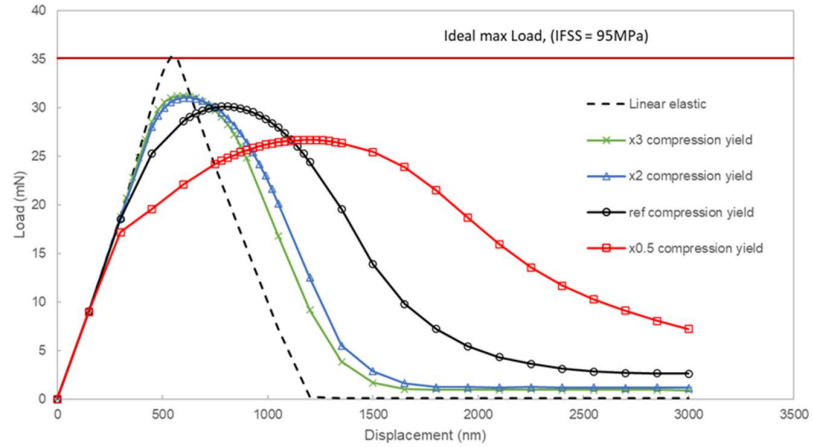

Figure 12: Effects of compressive yield strength on fiber push-out load-displacement response.

As illustrated in Figures 11 & 12, matrix plasticity properties have a strong effect on the fiber push-out response. As expected, the response is linear for a linear elastic material model, followed by a load drop with linear softening. It is worth noting that the FE model represents an "ideal" and perfectly flat free-standing test sample, and therefore the load-displacement response in the FE analysis does not exhibit the initial non-linearity and compliance artifact found in typical test data due to imperfect geometry and contact conditions (Figure 4). When plasticity is included, the pre-peak and post peak response are highly non-linear, as illustrated. It is demonstrated that the IFSS material input in the cohesive contact model is only accurately estimated from the max peak load according to Equation (1) when a linear elastic matrix material is considered. The relative percentage error in the estimation of the IFSS parameter is 14.3% for the reference plasticity properties listed in Table 1.

3.3 Effects of mode II interfacial fracture toughness

The effects of mode II interfacial fracture toughness parameter G_{IIc} used in the cohesive contact model representing the fiber/matrix interface in the FE model are illustrated in Figures 13 & 14 for a linear elastic and baseline Drucker-Prager plasticity-damage matrix material model, respectively.

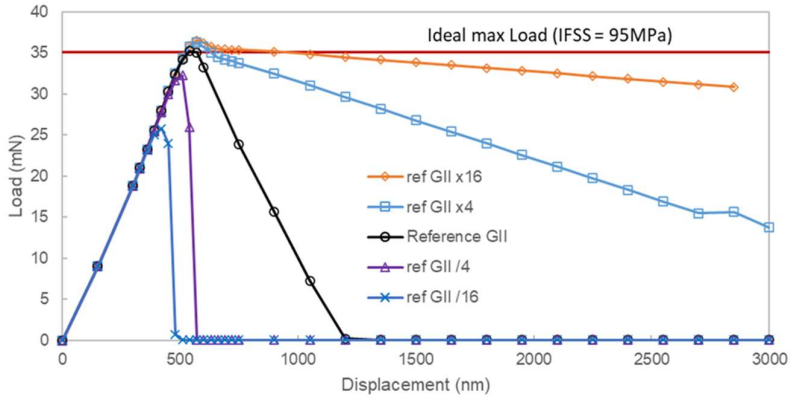

Figure 13: Effects of mode II interfacial fracture toughness on fiber push-out load-displacement response using a linear elastic matrix material model.

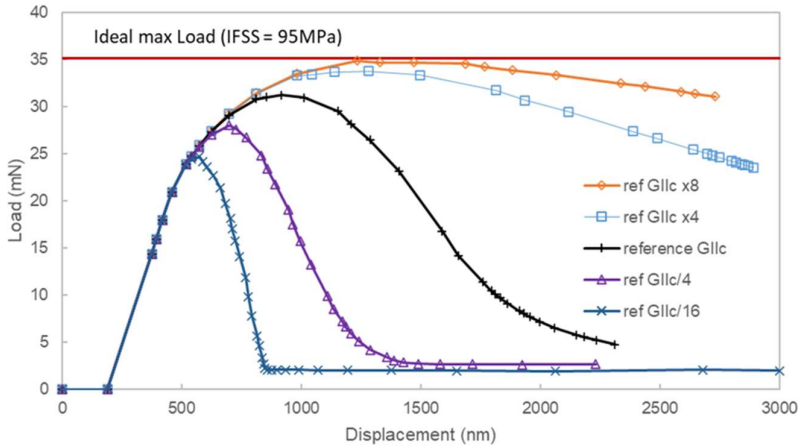

Figure 14: Effects of mode II interfacial fracture toughness on fiber push-out load-displacement response using a Drucker-Prager plasticity-damage matrix material model.

Results in Figure 13 for a linear elastic matrix material model show that the IFSS parameter can be accurately estimated from the peak load according to Equation (1) for sufficiently high values of the mode II fracture toughness energy (ductile fracture). For a low fracture toughness and brittle failure, the fracture toughness becomes the driving parameter and the peak load is not related to the IFSS parameter according to the closed-form solution. For a fracture toughness 16 times smaller than the reference value, the error in estimation of the IFSS input from the peak load is about 26%.

Results in Figure 14 for a non-linear matrix material model with plasticity damage show similar trend, with a lower peak load for low fracture toughness energy values. However, it is worth noting that convergence of the peak load with higher fracture toughness values is not established. Combined effects of matrix plasticity and shear interfacial fracture energy are illustrated where higher fracture toughness can compensate the peak load reduction related to matrix plasticity, approaching the ideal peak load closed-form solution. Such combination of effects can make interpretation of the push-out results and evaluation of the interfacial shear strength challenging.

3.4 Effects of interfacial friction

The effects of interfacial friction at the fiber/matrix interface on the push-out response are considered using Abaqus built-in isotropic Coulomb friction in combination with cohesive contact. In this model, contribution from friction on interfacial shear stress is weighted by the scalar cohesive damage variable (0 for an undamaged interface and 1 for a fully damaged interface). Sensitivity to the friction coefficient is presented in Figures 15 & 16, for a linear elastic and baseline Drucker-Prager plasticity-damage matrix material model, respectively.

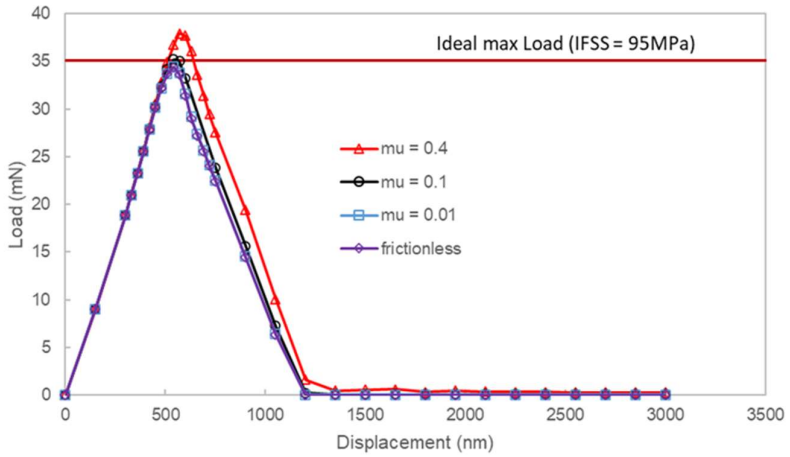

Figure 15: Effects of interfacial friction on fiber push-out load-displacement response using a linear elastic matrix material model.

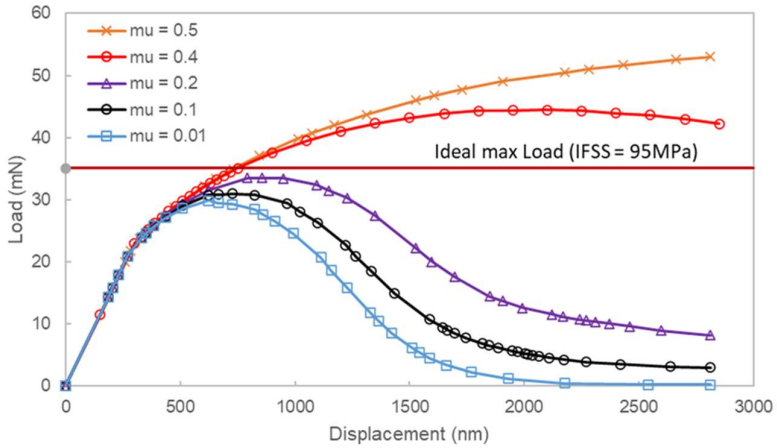

Figure 16: Effects of interfacial friction on fiber push-out load-displacement response using a Drucker-Prager plasticity-damage matrix material model.

As shown in Figure 15, the friction coefficient has relatively low influence on the maximum peak load and the push-out response for a linear elastic matrix material. An 8% increase in peak load is observed for a high friction coefficient μ = 0.4, but the shape of the load-displacement response is relatively unchanged. On the other hand, friction has a strong effect on both the maximum peak load and the shape of the load-displacement response when coupled with matrix plasticity, as illustrated in Figure 16.

3.4 Residual stress and sink-in deformation

FE analysis is used to substantiate the assumption that the matrix sink-in deformation observed in free-standing test specimens after a group of fibers is pushed-out is related to the release of residual stress. The analysis includes a curing analysis step, grinding/polishing step and fiber push-out step.

The curing analysis is carried out using Abaqus built-in material curing models and capabilities and includes a cure kinetics model, chemical shrinkage evolution, thermal expansion properties and dependency of the Young's modulus on temperature and degree of cure.

The cure kinetics model is implemented using the following form of the Kamal equation:

$$\dot{\alpha} = A_1 \exp\left(-\frac{\Delta E_1}{RT}\right)(1-\alpha)^n + A_2 \exp\left(-\frac{\Delta E_2}{RT}\right)\alpha^m(1-\alpha)^n \tag{2}$$

Where $\dot{\boldsymbol{\alpha}}$ is the rate of cure: $\boldsymbol{\alpha}$ is the degree of cure; $\boldsymbol{R}$ is the gas constant and T the temperature. $\boldsymbol{A_1, A2, m, n, \Delta E_1, \Delta E_2}$ are cure kinetics parameters obtained from fitting curing data provided by Schechter *et al* in Ref. [17] for 121°C cure F4A epoxy resin system and listed in Table 2.

Parameter	Value
m	1.21
n	2.70
A_1	2.32×10^{15} (s^{-1})
A_2	3.20×10^{7} (s^{-1})
ΔE_1	1.50×10^{5} (J/mol)
ΔE_2	6.99×10^{4} (J/mol)

Table 2: Cure kinetics parameters for F3G epoxy resin.

A linear model is used for the evolution of chemical shrinkage strain $\boldsymbol{\varepsilon^{chem}}$ as a function of degree-of-cure $\boldsymbol{\alpha}$:

$$\varepsilon^{chem} = \varepsilon_{100}^{chem}\alpha \tag{3}$$

$\boldsymbol{\varepsilon_{100}^{chem}}$ is a constant quantifying the final chemical shrinkage at 100% cure and a value of $\boldsymbol{\varepsilon_{100}^{chem}}$ = 3.45% is used based on in-house characterization.

The evolution of matrix Young's modulus under the prescribed cure cycle considered in the analysis is illustrated in Figure 17.

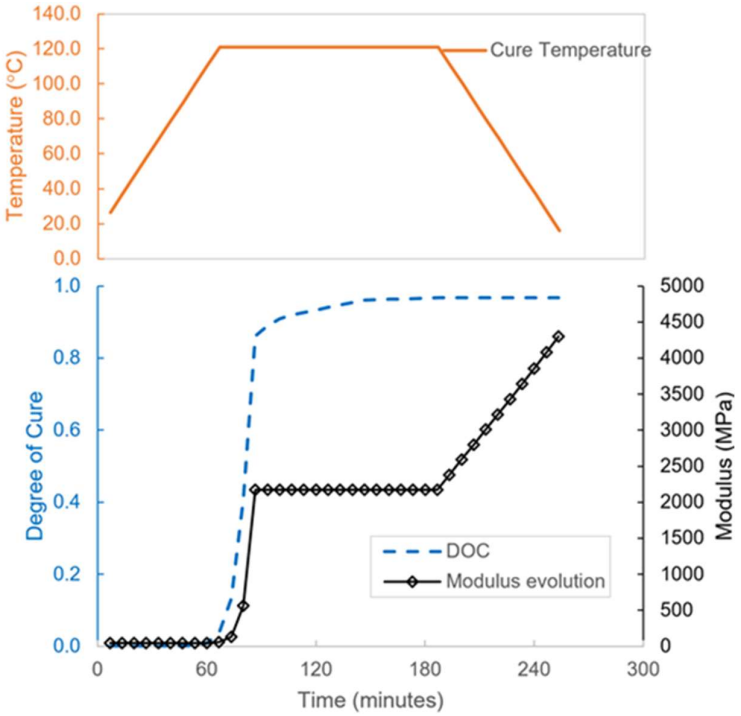

Figure 17: Cure cycle and modulus development for F3G epoxy matrix.

During the curing simulation, a symmetry boundary condition is applied on the top and bottom surfaces perpendicular to the fiber direction (Z surfaces), while the other surfaces (X & Y surfaces), are left unconstrained. The Z-symmetry boundary condition is relaxed during the polishing/grinding step using Abaqus native "model change" capabilities to replicate the material removal process used to achieve the final specimen membrane thickness. After the polishing step, the push-out process is simplified and modeled by modifying the contact properties at the fiber/matrix interface from tied contact to frictionless contact throughout an equilibrium step using Abaqus model change capabilities for Contact Pairs. A subsequent analysis step is used to apply an imposed displacement boundary condition on the fibers selected for push-out that corresponds to the indenter total displacement after initial contact.

Figure 18 shows the distribution of normal residual stress in the out-of-plane direction at the end of the curing simulation step. As illustrated, the matrix is under tensile stress. In this example, the average tensile residual stress in the matrix is 178 MPa. Figure 19 shows the out-of-plane deformation field after the polishing step (Figure 19a) and after pushing out a group of 8 fibers (Figure 19b). As illustrated, the FE analysis qualitatively reproduces the matrix "sink-in" deformation observed in test data (Figure 7) by capturing relaxation of cure-induced residual stress upon fiber push-out.

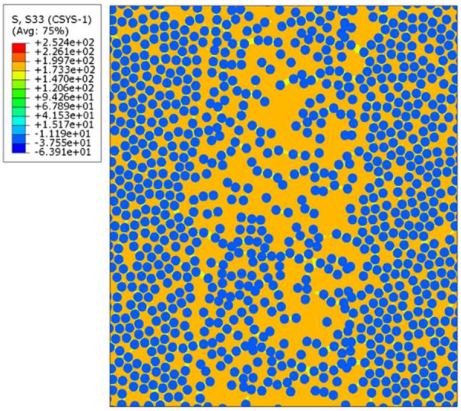

Figure 18: Distribution of normal residual stress in the out-of-plane direction at the end of the curing simulation step.

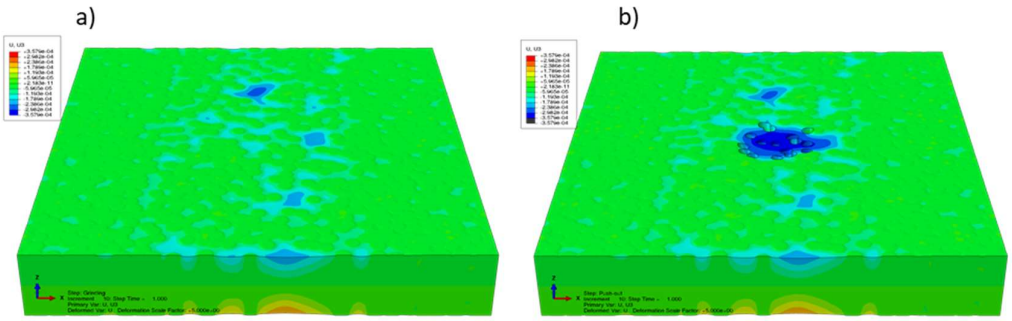

Figure 19: Out-of-plane displacement field a) after the polishing analysis step and b) after push-out simulation.

3.5 Effect of residual stress

The effects of residual stress on the fiber push-out response are evaluated by using the refined free-standing FE model with embedded mesh and simulation of the cure and polishing processes presented in the previous section. In this study, the individual fiber push-out is modeled by physically pushing the fiber with the contacting probe and simulating progressive debonding using the cohesive contact model as previously described. The load-displacement results for a linear and non-linear plastic matrix material model are presented in Figure 20. As shown in Figure 20, including residual stress in the analysis results in a lower peak load in the push-out response. However, it is worth noting that the decrease in the apparent IFSS value does not exceed 5%, which is a relatively small compared to the effects of other influencing factors evaluated previously, including matrix plasticity.

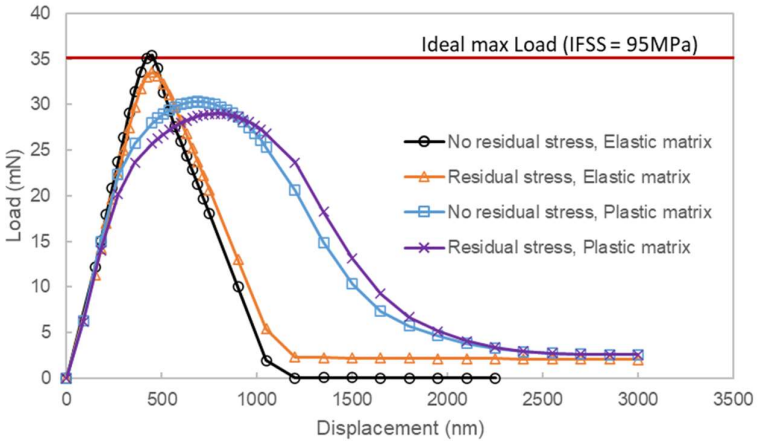

Figure 20: Effects of residual stress on fiber push-out load-displacement response for linear elastic and plasticity-damage matrix material models.

9 CONCLUSIONS

An experimental and numerical study was presented in this work with the objective to improve the understanding of fiber/matrix IFSS measurement using the push-out test.

Experimental push-out results for HM63/8552 carbon/epoxy material were compared between free-standing test specimens machined using a traditional grinding/polishing method and cave test specimens prepared using femtosecond laser ablation. Both test setups resulted in similar IFSS, indicating that the specimen preparation method did not affect the interfacial shear strength measurement in this case. However, free-standing test specimens showed increased sensitivity to test boundary conditions and geometric imperfections which could potentially result in unintended failure modes and interfere with characterization of the interfacial shear properties. Caves specimens are free of such imperfections and seem to be better-suited candidates for assessment of the fiber-matrix interface shear response, including the interface strength.

In-situ SEM-based fiber push-out experiments were presented where significant permanent matrix sink-in deformation was observed after groups of neighboring fibers in resin rich areas are pushed-out, which was associated with the release of process-induced residual stress. The maximum deformation was measured at 1.0-1.6% of specimen thickness, which is significant, suggesting high levels of residual stress.

A numerical FE study was conducted to evaluate the effects of multiple material properties on direct measurement of IFSS in a carbon-epoxy material system, including matrix plasticity, interface mode II fracture toughness and interfacial friction. It was shown that direct evaluation of the IFSS using the maximum peak load recorded in the push-out response is only accurate for a linear elastic matrix material response with relatively ductile interface fracture behavior and low coefficient of interfacial friction.

Finally, a FE analysis procedure was presented to include the effects of cure-induced residual stress in the fiber push-out simulation. The analysis was able to replicate the matrix sink-in deformation observed experimentally when a group of neighboring fibers in a resin-rich area are pushed-out. Residual stress generated in the analysis were found to have an effect on the apparent IFSS value (conservative by 5%); however, this effect was relatively small compared to potential effects of other influencing factors, including matrix plasticity.

ACKNOWLEDGEMENTS

This research was partially funded by the U.S. Government under Agreement No. W911W6-17-2-0002. Such support is gratefully acknowledged. The U.S. Government technical monitor is Mahendra Bhagwat. The views and conclusions contained in this document are those of the authors and should not be interpreted as representing the official policies, either expressed or implied, of the U.S. Government.

REFERENCES

[1] A. Makeev , S. Ghaffari and G. Seon, Improving compressive strength of high modulus carbon-fiber reinforced polymeric composites through fiber hybridization, *International Journal of Engineering Science*, **142**, 2019, pp. 145-157 (https://doi.org/10.1016/j.ijengsci.2019.06.004)

[2] S. Ghaffari, A. Makeev, G. Seon, D. P. Cole, D. J. Magagnosc and S. Bhowmick, Understanding compressive strength improvement of high modulus carbon-fiber reinforced polymeric composites through fiber-matrix interface characterization, *Materials & Design*, **193**, 2020, p.108798 (https://doi.org/10.1016/j.matdes.2020.108798)

[3] S. Ghaffari, G. Seon and A. Makeev, In-situ SEM based method for assessing fiber-matrix interface shear strength in CFRPs, *Materials & Design*, **197**, 2021, p 109242 (https://doi.org/10.1016/j.matdes.2020.109242)

[4] L. P. Canal, C. Gonzalez, J. Segurado and J. Llorca, Intraply fracture of fiber-reinforced composites: Microscopic mechanisms and modeling, *Composites Science and Technology,* **72**(2), 2012, pp. 1223-1232 (https://doi.org/10.1016/j.compscitech.2012.04.008)

[5] N. Chandra and H. Ghonem, Interfacial mechanics of push-out tests: theory and experiments, *Composites Part A: Applied Science and Manufacturing*, **32**, 2001, pp. 575-584 (https://doi.org/10.1016/S1359-835X(00)00051-8)

[6] S.-L. Gao and E. Mäder, Characterisation of interphase nanoscale property variations in glass fibre reinforced polypropylene and epoxy resin composites, *Composites Part A: Applied Science and Manufacturing*, **33**(4), 2002, pp. 559-576 (https://doi.org/10.1016/S1359-835X(01)00134-8)

[7] D. B. Marshall, An Indentation Method for Measuring Matrix - Fiber Frictional Stresses in Ceramic Composites, *The American Ceramic Society*, **67**(12), 1984, pp. C-259-C-260 (https://doi.org/10.1111/j.1151-2916.1984.tb19690.x)

[8] R. Young, C. Thongpin, J. Stanford and P. Lovell, Fragmentation analysis of glass fibres in model composites through the use of Raman spectroscopy, *Composites Part A: Applied Science and Manufacturing*, **32**(2), 2001, pp. 253-269 (https://doi.org/10.1016/S1359-835X(00)00091-9)

[9] S. Zhandarov and E. Mäder, Characterization of fiber/matrix interface strength: applicability of different tests, approaches and parameters, *Composites Science and Technology*, **65**(1), 2005, pp. 149-160 (https://doi.org/10.1016/j.compscitech.2004.07.003)

[10] X. -F. Zhou, H. D. Wagner and S. R. Nutt, Interfacial properties of polymer composites measured by push-out and fragmentation tests, *Composites Part A: Applied Science and Manufacturing*, **32**(11), 2001, pp. 1543-1551 (https://doi.org/10.1016/S1359-835X(01)00018-5)

[11] A. Salama, L. Li, P. Mativenga and A. Sabli, High-power picosecond laser drilling/machining of carbon fibre-reinforced polymer (CFRP) composites, *Applied Physics A*, **73**(122), 2016, pp. 1-11 (https://doi.org/10.1007/s00339-016-9607-8)

[12] E. Uhlmanna, G. Spur, H. Hocheng, S. Liebelt and C. T. Pan, The extent of laser-induced thermal damage of UD and crossply composite laminates, *International Journal of Machine Tools & Manufacture*, **39**, 1999, pp. 639-650 (https://doi.org/10.1016/S0890-6955(98)00045-5)

[13] B. Rohrmüller, P. Gumbsch and J. Hohe. Calibrating a fiber–matrix interface failure model to single fiber push-out tests and numerical simulations, *Composites Part A: Applied Science and Manufactur*, **150**, 2021, p. 106607 (https://doi.org/10.1016/j.compositesa.2021.106607)

[14] D.U. Shah and P.J. Schubel, Evaluation of Cure Shrinkage Measurement Techniques for Thermosetting Resins, *Polymer Testing*, 29, 2010, pp. 629–639 (https://doi.org/10.1016/j.polymertesting.2010.05.00)1

[15] L. Khoun and P. Hubert, Cure Shrinkage Characterization of an Epoxy Resin System by Two in Situ Measurement Methods, *Polymer Composites*, 2010, **31**, pp. 1603–1610 (https://doi.org/10.1002/pc.20949)

[16] J. Segurado and J. Llorca, A numerical approximation to the elastic properties of sphere reinforced composites, *Journal of the Mechanics and Physics of Solids*, **50**(10), 2002, pp.2107-2121 (https://doi.org/10.1016/S0022-5096(02)00021-2)

[17] S.G.K. Schechter, L.K. Grunenfelder and S.R. Nutt, Air Evacuation and Resin Impregnation iSemipregs: Effects of Feature Dimensions, *Advanced Manufacturing: Polymer & Composites Science,* **6**(2), 2020, pp. 101–114 (https://doi.org/10.1080/20550340.2020.1768348)